

Supporting Information

Surface-Passivated Plasmonic Nano-Pyramids for Bulk Heterojunction Solar Cell Photocurrent Enhancement

Alec Kirkeminde,[†] Markus Retsch,[‡] Qian Wang,[§] Guowei Xu,[⊥] Rongqing Hui,[§] Judy

Wu,[⊥] Shenqiang Ren^{†,}*

[†] Department of Chemistry, [§] Department of Electrical Engineering and Computer Science, [⊥] Department of Physics and Astronomy, University of Kansas, Lawrence, KS, USA 66045

[‡] Physical Chemistry I, University of Bayreuth, 95440 Bayreuth, Germany

1. Methods

Plasmonic-Based Organic Solar Cell Device Fabrication. The whole device structure consists of the following sequence of films and thicknesses: ITO/Au nanopyramids:poly(3,4-ethylenedioxythiophene)-poly(styrenesulfonate) (PEDOT-PSS) (30 nm)/ P3: PCBM (70 nm)/Al (120 nm). PEDOT:PSS (Baytron PVP CH 8000) is spin cast onto a 0.5×0.5 in² glass substrate with pre-patterned ITO electrodes. The PEDOT:PSS is useful as a hole transport layer and yields a smooth surface of ITO. The Au nanopyramids with different size and ligands were patterned onto the ITO substrate by a polystyrene (PS) based nanosphere lithography technique. The blended P3/PCBM in the 1,2-dichlorobenzene (1,2-DCB) solution is spun at 1000 rpm for 1 min, and subjected to 1,2-DCB solvent annealing overnight. The coated device was annealed at 140°C for 10 min, and then quickly cooled to room temperature. The 120 nm thick Al top contact layer was evaporated at a rate of 0.1 nm/s as the cathode, through a shadow mask to generate an array of patterned electrodes (the active photoactive area is 0.01 cm²). The final device area was defined by the overlap between the top and bottom electrodes.

Plasmonic Simulation of Au Nanopyramid. To confirm the plasmonic effect, we have performed a *Finite-Difference Time-Domain* (FDTD) simulation based on *FULLWAVE* simulation package from R-Soft Inc. The simulation used an ideal Au nanopyramid with 30nm thickness and 110nm bottom side lengths. The Au nanopyramid was placed on the front surface of the semi-infinite ITO substrate, and a plane lightwave was normally launched with a single polarized electrical field E_x . The simulation area was 200nmX200nm in the horizontal dimension. Perfectly matched layer (PML) conduction was used for the boundary of simulation window which absorbs the energy without inducing reflections. Only one Au nanopyramid was included in the simulation area so that the simulation time was not too long, but as the consequence the effect of interference between different Au nanopyramid was not included. Optical power flow was integrated over a box surrounding the Au nanopyramid using the Q-calculation function of the simulation package, and the calculated Q value is proportional to the absorption cross section of the Au nanopyramids. The calculated plasmonic resonance wavelength is approximately 600nm for the Au nanopyramid.

Device Characterization. Current-voltage (J - V) characteristics of the finished devices are measured in a nitrogen atmosphere glovebox with a source-meter (Keithley 2400). There are 60 different solar cell devices for each condition (different sized Au nanopyramids) which have been tested for the photovoltaic performance. The J - V curves in the main text represent the average device performance, and at least 10 samples has been characterized for each surface passivated ligand on 110 nm Au NPYs. Sheet resistance values of the ITO anode in the presence and in the absence of Au NPYs were evaluated using four-point-probe method. The light response was measured under illumination from a 100mW/cm² AM1.5 solar simulator. Transmittance and absorbance spectra of the device active layer were measured with a Shimadzu UV-3600 UV-Vis-NIR dual-beam spectrophotometer. To measure the hemispherical transmittance of a plasmonic sample, a Labsphere RTC 060 SF integrating sphere is used which collects the transmitted irradiance scattered in all hemispherical directions.

Structural Characterization. Surface morphology of the organic solar cell devices was investigated using Digital Instruments Dimension 3000 atomic force microscope (AFM) operating in tapping mode. The plan-view and cross-sectional images of Au nanopyramid structures were studied using the LEO 1550 field emission scanning electron microscope (SEM) at 10 KV.

2. Narrow band gap conjugated polymer P3

In this study, we focused on the plasmonic effect on the photovoltaic response of narrow bandgap organic solar cells, and the synthesis of conjugated polymer P3 will be discussed in the future report. In the P3 polymer (Figure s1, $x=1$), the silole shows higher hole mobility and better crystalline compared to their carbon analogues.^{1,2} The 3-hexyl-thiophene based unit is used for the enhanced packing. The absorption can be tuned by increasing the length of thiophene unit (x). The mobility μ of conjugated polymer P3 is 3.5*10⁻⁵ cm²/Vs, 1*10⁻⁴ cm²/Vs, without annealing and with annealing at 140 °C, respectively.

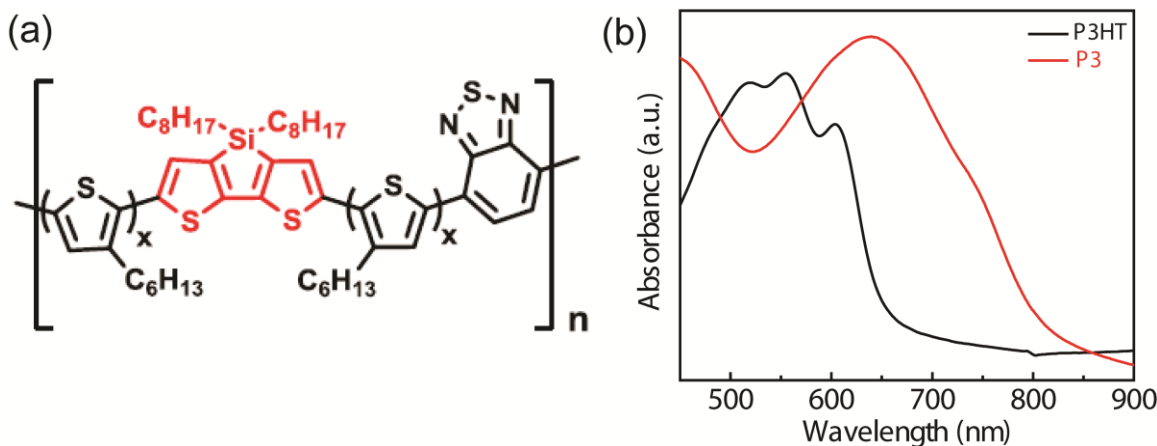


Figure S1. (a) The schematic diagram of conjugated polymer P3 structure, when $x=1$. (b) The photoabsorption spectrum of P3 and P3HT conjugated polymer.

3. *J-V* Characterization of Solar Cells with and without Au Nanopyramids

The effect of nanoplasmonic on the photocurrent properties of photoactive P3/PCBM films was demonstrated by the DC current density (J)–voltage (V) characteristics of the non-plasmonic (Figure S2a) and plasmonic (Figure S2b) devices. The plasmonic-based solar cell device consisted of self-assembled Au nanopyramids (110 nm side length) with SH-PEG ligands embedded with PEDOT:PSS, P3/PCBM and Al layers. As shown in Figure S2b, the plasmonic device shows a strong enhancement of photocurrent over the non-plasmonic device. This result is again consistent with the fact that the nanoplasmonics enhances the light absorption and charge separation in the P3/PCBM phase. Figure S2c shows the diffuse reflectance spectra of the devices fabricated with and without the Au nanopyramids in P3/PCBM photovoltaic devices using the integrated sphere technique. The slightly lower reflectivity of the devices with Au nanopyramids indicates enhanced transmission and absorption of the incident light.

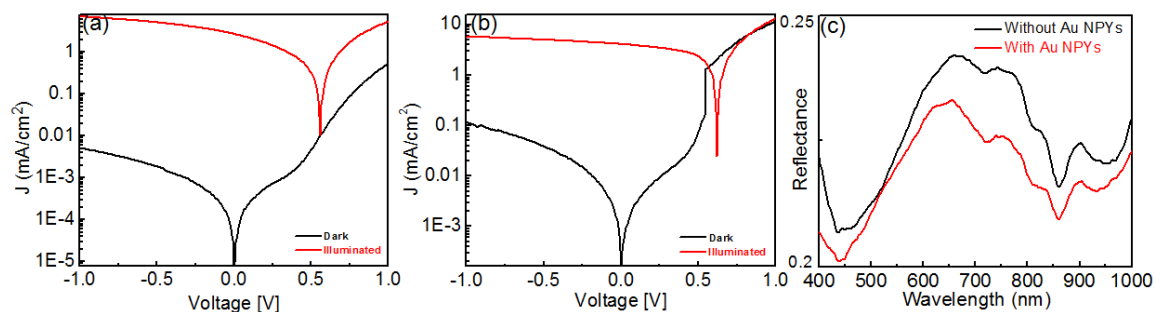


Figure S2. (a) J - V characteristics of non-plasmonic cell measured with incident light intensities from 100 mW/cm^2 AM 1.5 solar simulator. (b) J - V characteristics of a Au nanopyramid plasmonic solar cell measured with incident light intensities from 100 mW/cm^2 AM 1.5 solar simulator. (c) Diffuse reflectance spectra of the devices fabricated with P3/PCBM bulk heterojunction photovoltaics (black curve) and Au nanopyramid plasmonic P3/PCBM bulk heterojunction photovoltaics (red curve).

The light intensity dependent photovoltaic performance was examined shown in Figure S3. Generally, increasing incident light intensity can increase the generated photocurrent as well as the efficiency of solar cells (Figure S3a). A near-linear shape is demonstrated in the short circuit current-intensity relation, and the fill factor (FF) and open circuit V_{oc} get saturated at a low light intensity (Figure S3b and S3c), showing the geminate recombination mechanism.^{3,4} Linear relationship between J_{sc} and light intensity may, on the other hand, show a combined result of both the linear light absorption increase of the photoactive layer and the plasmonic induced linear light absorption enhancement when the incident light intensity increases. If this is the case, the plasmonic effect will be excited even further and effectively influence the light absorption of the above photoactive layer, improving the performance of organic solar cells.

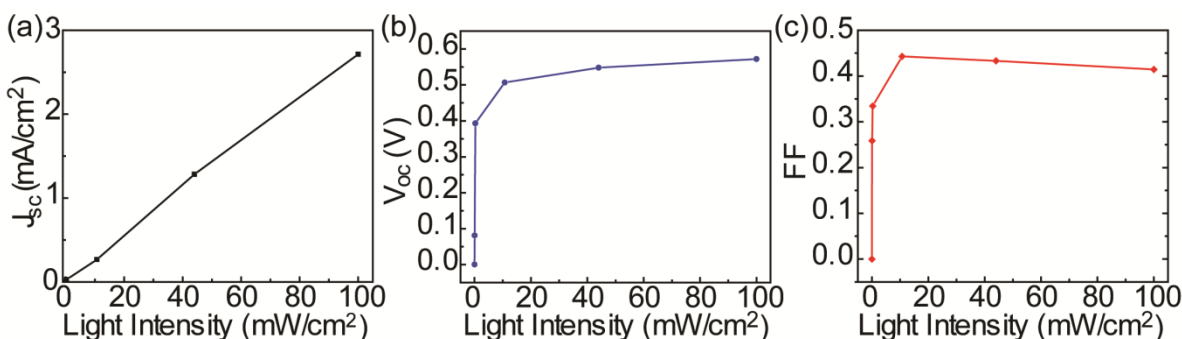


Figure S3. (a) Light intensity photovoltaic performance study which shows a linear trend. (b) Light intensity's effect on open circuit voltage showing a stable trend as intensity increases. (c) Light intensity's effect on fill factor number shows a stable trend as intensity increases.

Table s1. Series resistance (R_s) of devices with different Sized Au Nanopyramids. In order to provide a deeper insight into the sheet resistance of the anode on the PV effects, series resistances (R_s) are analyzed. R_s arises from the power loss of various resistive layers in PV devices and is given by

$$R_s A = (L^2 R_{\text{sheet anode}}) / 3 + (\rho t)_{\text{PEDOT:PSS}} + (\rho t)_{\text{P3:PCBM}}$$

where A is the active area, $R_{\text{sheet anode}}$ is the sheet resistance of anode, L is the length of P3/PCBM PV device, ρ and t are the resistivity and thickness of the organic layers.⁵ The sheet resistance of the ITO anode does not reduce significantly in the presence of the different sized Au nanopyramids, 111.2 (bare ITO), 102.2 (55-nm side Au NPYs-ITO), 96.1 (80-nm side Au NPYs-ITO), 92.4 (110-nm side Au NPYs-ITO), and 90.2 (225-nm side Au NPYs-ITO) $\Omega \text{ cm}^2$, which are evaluated using four-point-probe method. The R_s values attained from $J_D - V$ data of devices are much larger than that measured from the anode sheet resistance. The R_s values suggest that the total resistive power loss in the PV device is governed by the P3:PCBM layer.

anode morphology	series resistance (Ω/cm^2)
Bare ITO	660
55-nm size Au Nanopyramid-ITO	546
80-nm size Au Nanopyramid-ITO	440
110-nm size Au Nanopyramid-ITO	332
225-nm size Au Nanopyramid-ITO	443

4. SEM Side-View of Au Nanopyramid Morphology

The side-view image of Au nanopyramid is represented in the Figure S4a, which shows the Au shape and dimensions. In combination with AFM surface morphology profile, it gives each Au nanopyramid size for the plasmonic simulation.

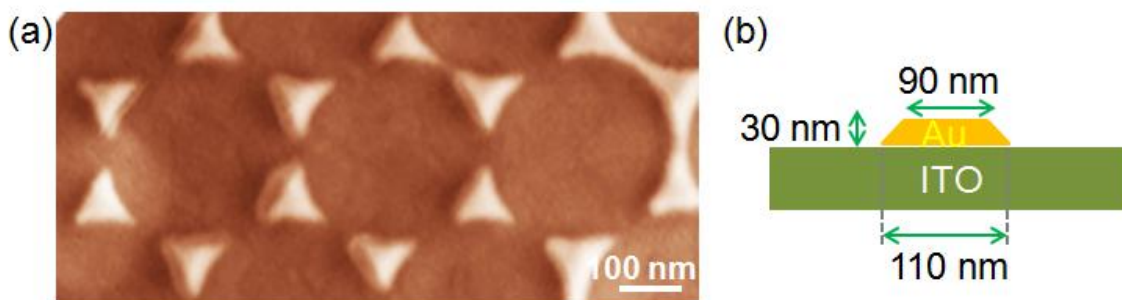


Figure S4. Side-view SEM image of the self-assembled Au nanopyramids on the patterned ITO substrate.

References:

- ¹ Lu, G.; Usta, H.; Risko, C.; Wang, L.; Facchetti, A.; Ratner, M. A.; Marks, T. J. *J. Am. Chem. Soc.* **2008**, *130*, 7670-7685.
- ² Hutchison, G. R.; Ratner, M. A.; Marks, T. J. *J. Am. Chem. Soc.* **2005**, *127*, 16866-16881.
- ³ Ren, S. Q.; Zhao, N.; Crawford, S. C.; Tambe, M.; Bulović, V.; Gradečak, S. *Nano Lett.* **2011**, *11*, 408-413.
- ⁴ Marsh, R. A.; McNeill, C. R.; Abrusci, A.; Campbell, A. R.; Friend, R. H. *Nano Lett.* **2008**, *8*, 1393-1398.
- ⁵ Choi, S.; Potscavage, W. J.; Kippelen, B. *J. Appl. Phys.* **2009**, *106*, 054507-10.